Journal of Cerebral Blood Flow & Metabolism (2015) 35, 623–629

www.jcbfm.com

ORIGINAL ARTICLE

Reference region modeling approaches for amphetamine challenge studies with [^{11}C]FLB 457 and PET

Christine M Sandiego[1,2], Jean-Dominique Gallezot[2], Keunpoong Lim[2], Jim Ropchan[2], Shu-fei Lin[2], Hong Gao[2], Evan D Morris[2] and Kelly P Cosgrove[1,2]

Detecting fluctuations in synaptic dopamine levels in extrastriatal brain regions with [^{11}C]FLB 457 and positron emission tomography (PET) is a valuable tool for studying dopaminergic dysfunction in psychiatric disorders. The evaluation of reference region modeling approaches would eliminate the need to obtain arterial input function data. Our goal was to explore the use of reference region models to estimate amphetamine-induced changes in [^{11}C]FLB 457 dopamine D2/D3 binding. Six healthy tobacco smokers were imaged with [^{11}C]FLB 457 at baseline and at 3 hours after amphetamine (0.4 to 0.5 mg/kg, per os) administration. Simplified reference tissue models, SRTM and SRTM2, were evaluated against the 2-tissue compartmental model (2TC) to estimate [^{11}C]FLB 457 binding in extrastriatal regions of interest (ROIs), using the cerebellum as a reference region. No changes in distribution volume were observed in the cerebellum between scan conditions. SRTM and SRTM2 underestimated binding, compared with 2TC, in ROIs by 26% and 9%, respectively, with consistent bias between the baseline and postamphetamine scans. Postamphetamine, [^{11}C]FLB 457 binding significantly decreased across several brain regions as measured with SRTM and SRTM2; no significant change was detected with 2TC. These data support the sensitivity of [^{11}C]FLB 457 for measuring amphetamine-induced dopamine release in extrastriatal regions with SRTM and SRTM2.

Journal of Cerebral Blood Flow & Metabolism (2015) **35,** 623–629; doi:10.1038/jcbfm.2014.237; published online 7 January 2015

Keywords: amphetamine challenge; C-11 FLB 457; D2/D3 receptors; extrastriatal dopamine; PET; reference region

INTRODUCTION

Nicotine and other drugs of abuse exert their rewarding, reinforcing, and motivational effects through the mesolimbic and mesocortical dopamine systems.[1] Striatal dopamine changes have been reliably detected using positron emission tomography (PET) with dopamine D2/D3 radiotracers, such as [^{11}C]PHNO and [^{11}C] raclopride, after an amphetamine challenge.[2–4] The ability to measure changes in extrastriatal dopamine levels, including thalamus, amygdala, prefrontal cortex, as well as other cortical areas, is useful for further advancing our understanding of the neuronal mechanisms that underlie addictive disorders.[5]

The high-affinity radiotracer [^{11}C]FLB 457, 5-bromo-N-[[(2S)-1-ethyl-2-pyrrolidinyl]methyl]-3-methoxy-2-(methoxy-^{11}C) benzamide has shown sensitivity and reliability for measuring amphetamine-induced dopamine release at extrastriatal dopamine D2/D3 receptors when adhering to scan constraints, such as mass limits $< \sim 0.6\,\mu g$ and collection of emission data for at least 90 minutes after radiotracer injection.[6,7] Another proviso is that the quantification of amphetamine-induced changes using reference tissue-input based models may lead to an underestimation in nondisplaceable binding potential (BP_{ND}),[8] as compared with arterial-input based models. The attractive feature of reference tissue modeling approaches is the circumvention of collecting arterial blood samples, a process that is invasive, may cause the subject discomfort, and is not always attainable. However, for reference region modeling the reference region should be validated for a given radiotracer with a displacement study to ensure the lack of specific binding. For radiotracers that target dopamine D2/D3 receptors using radioligands with moderate affinity, the cerebellum is typically used as the reference region due to a negligible amount of D2/D3 receptors that can be displaced (i.e., nondisplaceable = free and nonspecifically bound).[9]

Some studies with [^{11}C]FLB 457 have reported a reduction in cerebellum distribution volume, V_T(CER), postD2 antagonist or postpsychostimulant challenge, suggesting specific binding in the cerebellum.[10–12] A more recent [^{11}C]FLB 457 blocking study with aripiprazole (D2/D3 partial agonist) was performed to evaluate the fractional contribution to specific D2/D3 binding in the cerebellum, in addition to the pons and centrum semiovale (CESVL), to assess potential reference regions.[13] The change in V_T before and after aripiprazole was lower in the CESVL (−3%) and the pons (−10%), compared with the cerebellum (−17%). However, a reevaluation of previous data yielded lower variability with test-retest and amphetamine-induced changes in BP_{ND} and greater sensitivity to detect amphetamine-induced DA release across regions when V_T(CER) was used to estimate the nondisplaceable distribution volume, V_{ND}, compared with V_T(PONS) and V_T(CESVL). Other studies have supported reference region modeling approaches for the analysis of [^{11}C]FLB 457 BP_{ND} for low D2/D3 density regions,[14–17] but the degree of underestimation with amphetamine challenge studies and the sensitivity for detecting amphetamine-induced dopamine release, as compared with arterial input model methods, has not been examined.

[1]Department of Psychiatry, Yale University, New Haven, Connecticut, USA and [2]Department of Diagnostic Radiology, Yale University, New Haven, Connecticut, USA. Correspondence: Dr CM Sandiego, PET Center, Yale School of Medicine, PO Box 208048, New Haven, 06520-8048 CT, USA.
E-mail: christine.sandiego@yale.edu
This study was supported by NIDA grant K02DA031750 and the ORWH/NIDA grant P50DA033945.
Received 15 July 2014; revised 25 November 2014; accepted 30 November 2014; published online 7 January 2015

The aim of this study was to validate the use of reference region models for detecting changes in extrastriatal dopamine release because obtaining an arterial input function in human subjects is not always feasible. Our approach was to evaluate the simplified reference tissue models (SRTM), SRTM and SRTM2, with the 2-tissue compartmental model (2TC), for the analysis of [^{11}C]FLB 457 BP_{ND} before and after an amphetamine challenge in tobacco smokers. The change in cerebellum V_T was assessed, and the cerebellum was used to estimate BP_{ND} for each of the models across extrastriatal regions.

MATERIALS AND METHODS

Human Subjects

Positron emission tomography scans were performed in six tobacco smokers (4 male and 2 female, 39.5 ± 6.8 years old, 83.8 kg ± 13.7 kg). Written informed consent was obtained from all subjects. Subjects were medically and mentally healthy and were screened for the following: no current or history of medical illnesses, no prescription or illicit drug use, and based on psychiatric assessments (e.g., SCID and DSMIV Axis I) and mood measures (e.g., depression, anxiety, and impulsivity). Tobacco smoking inclusion criteria included: Fagerstrom Test for Nicotine Dependence of at least 3, smoking cigarettes daily for at least 1 year, and during intake evaluation, carbon monoxide levels greater than 8 p.p.m., plasma nicotine and cotinine levels greater than 10 and 50 ng/mL, respectively. Across subjects, cigarettes smoked per day and number of years smoked were 13.3 ± 5.2 and 20.8 ± 4.2, respectively. Females had negative pregnancy tests at intake and on the day of the scan. Approval for the study protocol was obtained from The Human Investigation Committee, Yale University School of Medicine, and Yale-New Haven Hospital Radiation Safety. The conducted study adhered to the Protection of Human Subjects of Research and Ethical Principle and Guidelines.

Each subject participated in two [^{11}C]FLB 457 PET scans on the same day, one baseline scan and one scan 3 hours after amphetamine administration. On a separate day, each subject had one MR scan, required to delineate anatomic information from the PET data.

Radiosynthesis of [^{11}C]FLB 457

[^{11}C]CO_2 was produced by a 16.5-MeV GE PETtrace cyclotron with 60 μA irradiation of a nitrogen target for 40 minutes. The [^{11}C]CO_2 was first converted to [^{11}C]methyl iodide then converted to [^{11}C]methyl triflate with either GE FXC Pro or Upgrade synthesis modules. The [^{11}C]methyl triflate, under helium stream, was bubbled into a solution of FLB 604 (0.3 to 0.6 mg), 5N NaOH (8 μL), and acetone (400 μL). The reaction proceeded for 5 minutes at room temperature, then the solution was diluted with 1 mL deionized water and injected onto a reverse-phase HPLC column (Phenomenex Prodigy ODS, 250 × 10 mm, 10 μm particle size). Using a mobile phase of 25% acetonitrile, 75% 0.1 mol/L ammonium formate, containing 0.03% ascorbic acid (pH 4.2) at a flow rate of 5 mL/min, the radioligand eluted and was collected after 16 to 17 minutes. The collected fraction was diluted with 50 mL deionized water containing 400 mg ascorbic acid. The diluted product was trapped on a Waters C18 Sep-Pak (Milford, MA, USA) and washed with 10 mL deionized water containing 10 mg ascorbic acid. The final product was eluted from the Sep-Pak using 1.0 mL of absolute ethanol (USP) and diluted with 10 mL of 0.9% sodium chloride (for injection, USP). The average specific activity was 978.0 ± 473.9 MBq/nmol (26.4 ± 12.8 mCi/nmol, $n = 12$) at end-of-synthesis, with chemical and radiochemical purities of ⩾ 93% and ⩾ 97%, respectively.

Input Function and Free Fraction Measurements

The arterial input functions were collected for all scans and were corrected for the presence of radiometabolites. For the first 7 minutes after injection, an automated blood counter (PBS-101; Veenstra Instruments, Joure, The Netherlands) with a peristaltic pump at a rate of 4 mL/min was used to measure the radioactivity continuously in whole blood. Manual sequential blood samples were also drawn (2 to 10 mL) at 3, 5, 7 , 10, 15, 20, 30, 50, 50, 60, 70, and 90 minutes after injection. The radioactivities of manual whole blood and plasma obtained from each corresponding sample via centrifugation (2,930 *g* at 4°C for 5 minutes) samples were counted in a cross-calibrated gamma counter (1480 WIZARD; Perkin-Elmer, Waltham, MA, USA). The plasma time-activity curve (TAC) was merged and extrapolated from these two sets of data. The end of the total plasma curve was fitted to a sum of exponentials to reduce noise in the input function.

Radiometabolites were measured in the plasma from arterial blood samples collected at 5, 15, 30, 60, and 90 minutes after injection using the automatic column-switching HPLC method[18] to determine the parent fraction. Plasma samples were initially treated with urea (8 mol/L), and then loaded onto a capture column (19 mm × 4.6 mm) packed with Phenomenex SPE C18 Strata-X sorbent and eluted with 1% acetonitrile in water at 2 mL/min. At 4 minutes, the activity trapped on the capture column was back-flushed onto an analytical HPLC column (Phenomenex Luna Phenyl hexyl, Torrance, CA, USA; 5 μm, 250 mm × 4.6 mm) eluted with 34% acetonitrile in 0.1 mol/L ammonium formate at 1.70 mL/min. An automated fraction collected the HPLC eluent and was counted in the gamma well counter. The parent fraction (retention time of ~10.5 minutes) was determined as the ratio of the sum of radioactivity containing the parent to the total amount of radioactivity. Parent fraction data were fitted with an inverted gamma function for five subjects and with a bounded sum of exponentials for one subject, as determined by the quality of fit. The arterial input function was calculated as the product of the fitted total plasma curve and the fitted parent fraction curve.

To measure the unbound portion, or free fraction (f_P), of [^{11}C]FLB 457, an ultrafiltration-based method was used. [^{11}C]FLB 457 (~7.4 MBq) was mixed with arterial blood (6 mL) drawn immediately before tracer injection. After 10 minutes at room temperature, the spiked blood sample was centrifuged at 2,930 *g* for 5 minutes to separate the plasma. Plasma aliquots (0.3 mL) were loaded onto the reservoir of the EMD Millipore Centrifree ultrafiltration device (Billerica, MA, USA) in triplicate and centrifuged at 1,228 *g* for 20 minutes. Free fraction was determined by calculating the ratio of the radioactivity concentration in the ultrafiltrate to the total activity in plasma. The amount of nonspecific binding of [^{11}C]FLB 457 to the filter was determined, as described above, by spiking the sample of saline with [^{11}C]FLB 457. The ultrafiltrate to spiked saline ratio was 97.51 ± 0.86 ($n = 12$), indicating negligible filter retention.

Amphetamine Administration and Plasma Levels

Amphetamine (0.4 to 0.5 mg/kg, PO) was administered 3 hours before the second [^{11}C]FLB 457 injection. Blood samples were collected to measure plasma amphetamine levels before amphetamine administration, $t = -180$ minutes, and at −120, −60, 0, 45, and 90 minutes, relative to the start time of the second [^{11}C]FLB 457 injection ($t = 0$ minute).

Positron Emission Tomography Scans and Image Reconstruction

Positron emission tomography scans were performed on the ECAT EXACT HR+ (Siemens/CTI, Knoxville, TN, USA). Before each radiotracer administration, a 6-minute transmission scan was acquired, necessary for attenuation correction of the PET emission data. [^{11}C]FLB 457 was injected intravenously as a bolus over 1 minute by a computer-controlled pump (Harvard Apparatus, Holliston, MA, USA), and emission data were collected for 90 minutes.

Emission data were collected and sinograms were reconstructed with all corrections (attenuation, normalization, scatter, randoms, and deadtime) into a sequence of 27 frames: 6 × 30 seconds; 3 × 1 minutes; 2 × 2 minutes; 16 × 5 minutes. Final image dimension and voxel size were 128 mm^3 × 128 mm^3 × 63 mm^3 and 2.06 mm^3 × 2.06 mm^3 × 2.43 mm^3, respectively. Motion correction on the dynamic data was performed by registering each frame to an early frame (i.e., the first 10 minutes after injection) using a 6-parameter mutual information algorithm (FMRIB's Linear Image Registration Tool, FMRIB Software library, version 3.2).[19]

Magnetic Resonance Scanning and Processing

T1-weighted magnetic resonance (MR) images were acquired on a 3T Trio whole-body scanner (Siemens Medical Systems, Erlangen, Germany) with a circularly polarized head coil. The final MR image dimension and pixel size were 256 mm^3 × 256 mm^3 × 176 mm^3 and 0.98 mm^3 × 0.98 mm^3 × 1.0 mm^3, respectively. Postprocessing of the MR images included a skull- and muscle stripping procedure so that only the brain remained in the image field-of-view (FMRIB's Brain Extraction Tool, http://fsl.fmrib.ox.ac.uk/fsl/fslwiki/BET), before coregistration with the PET images.

Positron Emission Tomography Image Processing

Positron emission tomography images were aligned to the MR via a rigid registration with mutual information. Each MR image was normalized

to Montreal Neurological Institute space[20] using an affine linear plus nonlinear registration (Bioimage Suite 2.5, http://www.bioimagesuite.org/index.html), to extract regions-of-interest (ROIs) from the automated anatomic labeling (AAL) template.[21] The ROIs were then mapped from the AAL template to PET space via the two transformations (e.g., PET-MR and MR-AAL template) to compute TACs in the following regions: amygdala (0.71 cm^3), anterior cingulate cortex (4.14 cm^3), dorsolateral prefrontal cortex (11.83 cm^3), hippocampus (2.86 cm^3), occipital cortex (15.36 cm^3), orbitofrontal cortex (11.07 cm^3), parietal cortex (12.83 cm^3), temporal cortex (32.85 cm^3), thalamus (3.29 cm^3), and ventromedial prefrontal cortex (10.21 cm^3), and cerebellum (15.98 cm^3). The AAL template was used to divide the prefrontal cortex into dorsolateral, orbitofrontal, and ventromedial. The dorsolateral prefrontal cortex was defined by combining the frontal superior, frontal mid, and frontal inferior triangularis corresponding to Brodmann's areas 9 and 46.[22] The orbitofrontal cortex was delineated by combining the frontal superior medial orbital and frontal medial orbital regions, and the ventromedial prefrontal cortex was defined by combining the frontal superior orbital and frontal superior medial regions.

Tracer Kinetic Modeling

The 2TC,[23] SRTM,[9] and SRTM2[24] were used for the kinetic analysis of regional BP^8_{ND} [^{11}C]FLB 457 TACs. For 2TC, the volume of distribution (V_T) in each ROI was estimated using the tissue TAC and the metabolite-corrected arterial input function. With the cerebellum as the reference region BP_{ND}(2TC) was computed as

$$BP_{ND} = \frac{V_T(\text{ROI})}{V_T(\text{CER})} - 1, \quad (1)$$

where V_T(ROI) and V_T(CER) are the volumes of distribution in the ROI and the cerebellum region, respectively.

The cerebellum was the reference input function for SRTM and SRTM2, where BP_{ND} was computed as

$$BP_{ND}(\text{SRTM}) = R_1\frac{k_2'}{k_2} - 1. \quad (2)$$

Parameters R_1, k_2, and k_2' are estimated directly from SRTM, where k_2 (1/minute) and k_2' (1/minute) are the rate constants of tracer efflux to the blood from the tissue in the ROI and reference tissue, respectively. R_1 is the ratio of tracer influx from the blood to tissue in the ROI and reference tissue, K_1 and K_1' (mL/cm^3/min), respectively. For SRTM2 only R_1 and k_2 are estimated where k_2' was shared across ROIs for each scan using coupled fits, where the TACs are fit simultaneously.[25]

Using an approximation of noise-equivalent counts for each frame, the data were weighted in the fits.[26] The models were evaluated in terms of quality of fit to the data, and the F-test ($P < 0.05$) was used to determine whether the ROI TAC fits across scans were statistically different between SRTM (3-parameter per ROI) and SRTM2 (2-parameter per ROI and 1 global parameter) models. BP_{ND}(SRTM) and BP_{ND}(SRTM2) were compared with BP_{ND}(2TC), the standard for comparison. This analysis was limited to data points for which the standard error (SE) for 2TC BP_{ND}(2TC) was less than 20% (%SE = SE/BP_{ND} × 100), to include only reliable 2TC estimates of BP_{ND}.

Percent change in BP_{ND} (%ΔBP_{ND}) from baseline to amphetamine challenge was computed as

$$\%\Delta BP_{ND} = \left(\frac{BP_{ND}\ (\text{challenge})}{BP_{ND}\ (\text{baseline})} - 1\right) \times 100. \quad (3)$$

Data are reported as mean ± s.d. Statistical analysis within each group was performed with two-tailed, paired *t-tests* with $P < 0.05$, without correction for multiple comparisons.

RESULTS

Scan Parameters

There were no differences between baseline and postamphetamine scans in injected dose, injected mass, or specific activity. Plasma-free fraction (f_P) was significantly different between scan conditions ($P < 0.05$) (Table 1). In the cerebellum reference region, no significant change was observed in [^{11}C]FLB 457 V_T (−8 ± 10%) nor V_T/f_p (−1 ± 13%) between scan conditions (Table 1).

Table 1. Scan parameters for [^{11}C]FLB 457 ($n = 6$ subjects)

	Baseline	*Postamphetamine*
Injected dose (MBq)	334 ± 49	338 ± 58
Specific activity (MBq/nmol)	376 ± 178	407 ± 172
Injected mass (μg)	0.40 ± 0.15	0.37 ± 0.14
Plasma-free fraction (f_p)	0.33 ± 0.02	0.30 ± 0.02*
Cerebellum V_T /f_P (mL/cm^3)	10.8 ± 2.0	10.6 ± 1.4
Cerebellum V_T (mL/cm^3)	3.5 ± 0.7	3.2 ± 0.4

Specific activity was at time of injection. There was no significant difference between scan conditions except for plasma free (*$P < 0.05$).

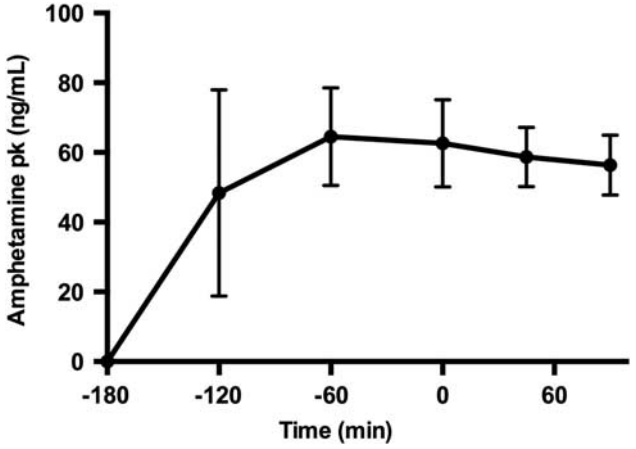

Figure 1. Amphetamine levels in the plasma (pk). Times are relative to the second [^{11}C]FLB457 injection at $t = 0$ minute. Data points are the mean across subjects ($n = 6$), and bars represent standard deviation.

Cerebellum V_T and V_T/f_p for each subject at baseline and postamphetamine challenge appear in Supplementary Figure 1.

Plasma Amphetamine Levels

Amphetamine levels peaked at 2 hours at 64.5 ± 14.0 ng/mL, remained elevated at the start of the second scan at 62.7 ± 12.5 ng/mL (3 hours after amphetamine), and were steady throughout the duration of the scan at 58.7 ± 8.5 ng/mL and 56.4 ng/mL ± 8.6 ng/mL (3 hours 45 minutes and 4 hours 30 minutes after amphetamine, respectively) (Figure 1). In one subject amphetamine levels peaked at 1 hour at 107.8 ng/mL, while the other subjects ranged from 30 to 45 ng/mL. In the same subject, the plasma level was 82.6 ng/mL at the start of scan 2 and remained ~10 to 20 ng/mL higher than the other 5 subjects for the duration of the scan.

Model Comparison

Model fits. All the models (2TC, SRTM, and SRTM2) produced good fits for low binding regions (Figure 2). Fit quality was slightly poorer for SRTM2, noticeably in the amygdala. On the basis of the F-test, [$F(9,240) = 1.92$, $P < 0.05$], SRTM had better fits across regions than SRTM2 for all scans.

Comparison of [^{11}C]FLB 457 BP_{ND} with reference region input models and 2-tissue compartmental model. SRTM and SRTM2 underestimated 2TC BP_{ND} for ROIs by 26% and 9%, respectively (Figure 3). The bias observed was driven mainly by higher-binding ROIs, the thalamus and amygdala. Bias across scan conditions was consistent, where baseline BP_{ND}(2TC) = 0.74BP_{ND}(SRTM) +0.20, $R^2 = 0.98$, and amphetamine challenge BP_{ND}(2TC) = 0.75

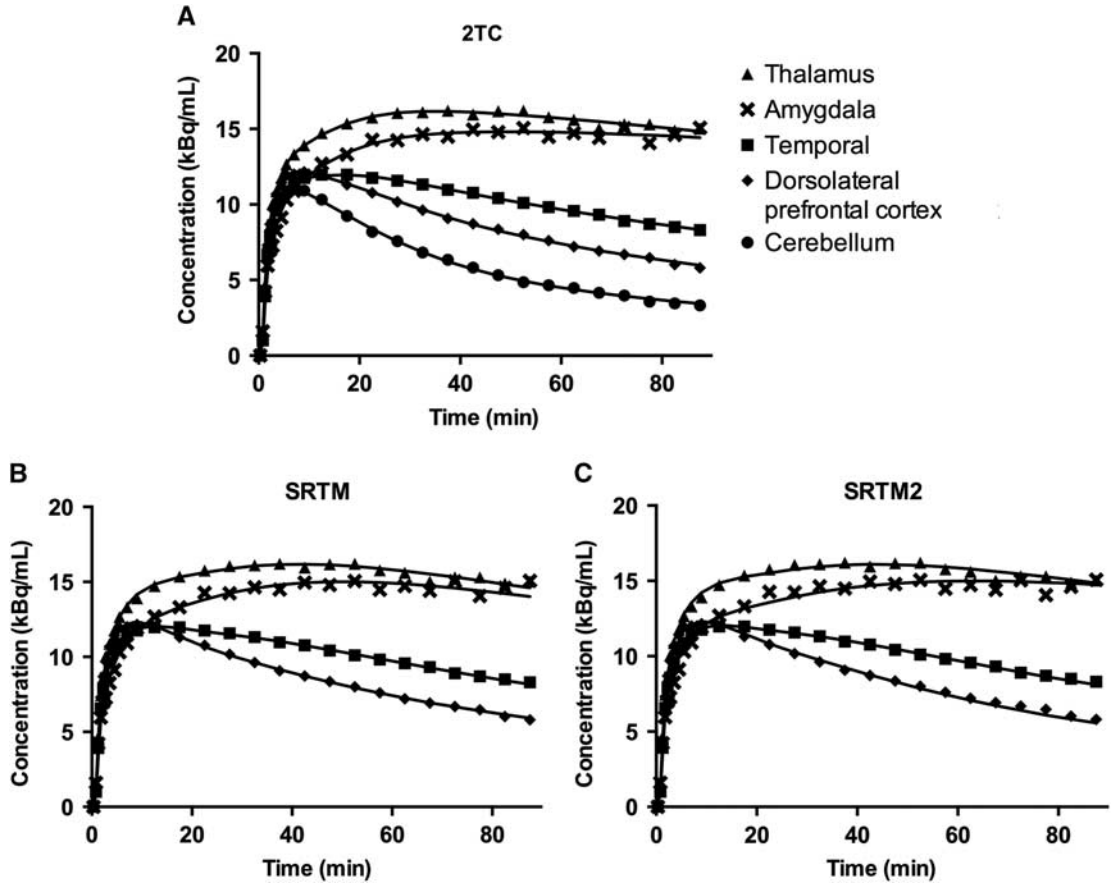

Figure 2. Typical regional time-activity curves from one representative subject and model fits for (**A**) 2-tissue compartmental model (2TC), (**B**) simplified reference tissue model (SRTM), (**C**) and SRTM2.

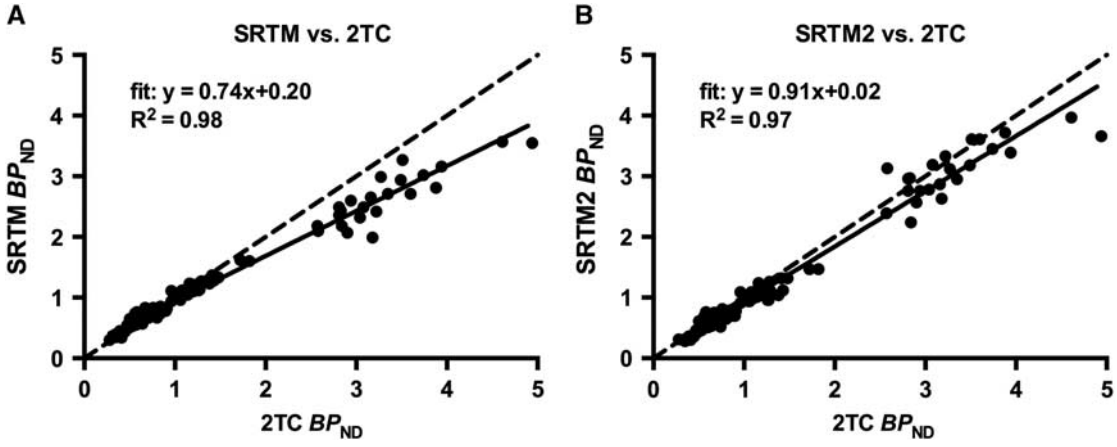

Figure 3. Model comparison of simplified reference tissue model (SRTM) and SRTM2 versus 2-tissue compartmental model (2TC) for [^{11}C]FLB 457 BP_{ND} for baseline and postamphetamine conditions in all ROIs evaluated. Both (**A**) SRTM and (**B**) SRTM2 underestimated 2TC BP_{ND} indicated with the regression fit (solid line). The identity plot (dashed line) was added for reference. Only 2TC BP_{ND} estimates with standard error $< 20\%$ were used in these comparisons.

BP_{ND}(SRTM)+0.16, $R^2 = 0.98$. Similarly, bias was consistent for BP_{ND}(SRTM2) across conditions, where baseline $BP_{ND}(2T) = 0.92$ BP_{ND}(SRTM2)+0.04, $R^2 = 0.96$, and amphetamine challenge $BP_{ND}(2T) = 0.90BP_{ND}$(SRTM2)+0.02, $R^2 = 0.98$. Due to the low intercept in the aforementioned regression equations, the bias induced by SRTM2 on the estimation of $\%\Delta BP_{ND}$, computed as

$1/1\left(1-\text{intercept}/\text{slope}/\text{BP}_{\text{ND}}^{\text{2TC}}\right)$, is expected to be lower than 5% in regions where the 2TC BP_{ND} is larger than 0.5.

Analysis of [^{11}C]FLB 457 %ΔBP_{ND} with 2-tissue Compartmental Model, Simplified Reference Tissue Model, and Simplified Reference Tissue Model 2

Model estimates of BP_{ND} and %ΔBP_{ND} for baseline and post-amphetamine challenge scans are shown in Table 2. With the 2TC model, mean %ΔBP_{ND} decreased nonsignificantly from the baseline to amphetamine challenge scans in the hippocampus, temporal cortex, and thalamus. Reductions in %ΔBP_{ND} were observed with SRTM and SRTM2 across all regions. With SRTM and SRTM2, BP_{ND} was reduced significantly ($P \leqslant 0.05$) postamphetamine in the amygdala, dorsolateral prefrontal cortex, hippocampus, and temporal cortex, and anterior cingulate cortex (SRTM2 only). Variability in %ΔBP_{ND} was smallest with SRTM2 in 6 of the 10 regions examined. For each subject, baseline and postamphetamine BP_{ND} values were plotted and shown in Supplementary Figure 2.

DISCUSSION

Positron emission tomography imaging studies can be complicated by the need to obtain arterial input functions. In human subjects, placement of arterial lines is invasive and not always attainable. In the current study, we compared reference region input modeling methods, SRTM and SRTM2, with the arterial input modeling method, 2TC, for the analysis of [^{11}C]FLB 457 BP_{ND} to determine the feasibility of analyzing the data using a reference region approach. Other reference region approaches, MRTM, MRTM2, and Logan (with different t^* values), were compared with 2TC for the analysis of BP_{ND}, evaluated preliminarily in the first four subjects' pre- and postamphetamine data sets. All approaches were negatively biased compared with BP_{ND}(2TC) and showed similar effects as SRTM and SRTM2. SRTM and SRTM2 estimates can be the least noisy due to lower number of parameters, compared with 2TC, or since all frame data points are included in fit, compared with MRTM, MRTM2, and Logan reference approaches. Thus, subsequent analyses of BP_{ND} were performed with SRTM and SRTM2.

The negative bias in BP_{ND} for SRTM and SRTM2, observed in Figure 3, is expected since SRTM works optimally for tracers that are well-fitted with the one-tissue compartment model, which is not the case for [^{11}C]FLB 457. When the gold standard is the 2TC model, it is expected that SRTM would introduce a bias, as seen for other tracers.[23,27,28] The amplitude of this bias would be different depending on the ROI properties: e.g., simulation studies with $5HT_{1A}$ radioligand [^{11}C]WAY-100635 showed that the negative bias with SRTM, using the cerebellum as reference input, is increased in regions with higher receptor density and with decreasing estimates of R_1 (ratio of tracer delivery rate to the target and reference ROI).[28] In this study, the bias was indeed larger in the higher binding thalamus and amygdala regions ($BP_{\text{ND}} > 2$), while the other ROIs with ($BP_{\text{ND}} < 2$) lay on the line of identity.

More importantly, the negative bias in BP_{ND} with SRTM (26%) and SRTM2 (9%) was consistent between baseline and post-amphetamine conditions such that the bias cancels out when computing the primary outcome measure, %ΔBP_{ND}. Postamphetamine reductions in BP_{ND} were observed with SRTM and SRTM2 across all regions examined, but not in all ROIs with 2TC. Additionally, SRTM and SRTM2 were more reliable models for detecting significant differences in BP_{ND} after the amphetamine challenge across several extrastriatal regions that were not detected with 2TC.

Table 2. [^{11}C]FLB457 BP_{ND} at baseline and postamphetamine challenge for 2TC, SRTM, and SRTM2 (mean ± s.d.)

	2TC				*SRTM*				*SRTM2*			
	Baseline	*Challenge*	*ΔBP_{ND}(%)*	P	*Baseline*	*Challenge*	*ΔBP_{ND}(%)*	P	*Baseline*	*Challenge*	*ΔBP_{ND}(%)*	P
Amyg	3.24 ± 0.49	3.22 ± 0.54	2.5 ± 29.5	0.957	2.52 ± 0.27	2.33 ± 0.18	−8.9 ± 6.4	0.021*	3.29 ± 0.33	2.84 ± 0.23	−13.4 ± 7.5	0.008*
Ant. cing.	1.01 ± 0.19	1.02 ± 0.19	0.8 ± 7.7	0.852	1.05 ± 0.17	1.03 ± 0.06	−8.5 ± 9.1	0.060	1.00 ± 0.18	0.94 ± 0.21	−6.7 ± 7.5	0.047*
Dlpfc	0.60 ± 0.15	0.62 ± 0.14	3.8 ± 12.5	0.603	0.68 ± 0.14	0.64 ± 0.11	−11.5 ± 8.7	0.008*	0.60 ± 0.15	0.56 ± 0.16	−7.3 ± 5.2	0.003*
Hipp	1.40 ± 0.17	1.25 ± 0.31	−11.6 ± 11.6	0.068	1.29 ± 0.17	1.23 ± 0.26	−12.9 ± 9.7	0.016*	1.14 ± 0.18	1.02 ± 0.25	−11.5 ± 9.5	0.023*
Occ	0.45 ± 0.14	0.48 ± 0.16	5.1 ± 9.7	0.327	0.52 ± 0.16	0.47 ± 0.11	−8.0 ± 14.7	0.223	0.45 ± 0.16	0.42 ± 0.18	−7.2 ± 12.0	0.213
Ofc	0.51 ± 0.14	0.54 ± 0.15	10.4 ± 39.0	0.722	0.56 ± 0.13	0.51 ± 0.16	−9.2 ± 22.5	0.389	0.49 ± 0.14	0.46 ± 0.16	−7.1 ± 13.7	0.375
Par	0.45 ± 0.14	0.50 ± 0.20	11.2 ± 19.7	0.313	0.53 ± 0.18	0.49 ± 0.12	−10.1 ± 16.3	0.282	0.46 ± 0.19	0.46 ± 0.22	−3.0 ± 12.6	0.892
Temp	1.14 ± 0.21	1.13 ± 0.25	−1.3 ± 7.1	0.781	1.12 ± 0.20	1.08 ± 0.21	−8.4 ± 8.1	0.036*	1.10 ± 0.21	1.02 ± 0.26	−7.7 ± 7.4	0.046*
Thal	3.61 ± 0.73	3.36 ± 0.77	−7.1 ± 6.9	0.057	2.99 ± 0.39	2.73 ± 0.44	−7.5 ± 8.5	0.084	3.26 ± 0.39	2.97 ± 0.65	−9.4 ± 10.7	0.097
Vmpfc	0.51 ± 0.17	0.54 ± 0.14	13.6 ± 22.3	0.211	0.58 ± 0.15	0.58 ± 0.06	−9.4 ± 12.9	0.084	0.51 ± 0.15	0.47 ± 0.17	−9.6 ± 18.7	0.186

Abbreviations: Amyg, amygdala; Ant. cing, Anterior cingulate cortex; Dlpfc, Dorsolateral prefrontal cortex; Hipp, Hippocampus; Occ, Occipital cortex; Ofc, Orbitofrontal cortex; Par, Parietal cortex; SRTM, simplified reference tissue model; Temp, Temporal cortex; Thal, Thalamus; Vmpfc, Ventromedial prefrontal cortex; 2TC, 2-tissue compartmental model. Significance level was *$P < 0.05$ (two-tailed, paired *t*-test, uncorrected for multiple comparisons) of the difference between baseline and postamphetamine challenge scans.

Plasma Amphetamine Levels

After amphetamine administration, plasma levels peaked at 2 to 3 hours for five subjects, however, one subject's plasma levels peaked early at 1 hour. This subject did not strongly influence the results when excluded from the analysis; ROIs with a significant decrease in BP_{ND} after amphetamine were retained. Importantly, at a dose of 0.4 or 0.5 mg/kg of amphetamine, plasma levels were consistent across subjects at the start of the second [^{11}C]FLB 457 scan.

Modeling Methods

All models visually produced good fits for low binding regions but were slightly poorer for SRTM2, more noticeable in the relatively higher binding regions. Statistically, SRTM produced better fits than SRTM2 across regions for all scans based on the F-test. However, compared with 2TC, SRTM2 was 17% less biased than SRTM for BP_{ND}. When comparing 2TC with SRTM, the frequency of cases where the relative standard error on BP_{ND} estimates exceeded 20% was 11% and 3%, respectively. Larger standard errors in BP_{ND} estimates are due to an increased number of parameters estimated with 2TC (4 parameters) versus SRTM (3 parameters). Another source of error in BP_{ND}(2TC) may be due to random fluctuations in arterial input function data. These factors that yield noise in BP_{ND}(2TC) may explain the lack of sensitivity to detect significant differences post-amphetamine, only 3 of the 10 ROIs examined had a mean reduction in BP_{ND}, and the larger variability in $\%\Delta BP_{ND}$ across subjects. On the basis of these data, reference region input modeling approaches decrease the noise in BP_{ND} estimates, increase the sensitivity to detect significant changes postamphetamine, and reduce the variability in $\%\Delta BP_{ND}$ across subjects.

Cerebellum as a Reference Region

Previous studies have reported specific binding of [^{11}C]FLB 457 in the cerebellum that would lead to an underestimation in BP_{ND}.[10–12] This underestimation applies to the 2TC model as well as to the SRTM and SRTM2 models, since 2TC BP_{ND} values were computed using the total V_T estimate for the cerebellum. Using the cerebellum as a reference in 2TC to compute BP_{ND} in amphetamine challenge studies induces a bias in the estimation of $\%\Delta BP_{ND}$. For example, if we assume that 17% of the cerebellum V_T correspond to specific binding,[13] then $\%\Delta BP_{ND}$ would be overestimated by ~25% (i.e., a true 16% decrease in the true BP_{ND} would lead to a $\%\Delta BP_{ND}$ estimate of −20%) in a region which true BP_{ND} is 1. This bias decreases in regions with larger true BP_{ND} (it would be ~11% in a region which true BP_{ND} is 2). Thus, this underestimation of BP_{ND} in 2TC leads to an overestimation of $\%\Delta BP_{ND}$.

Other studies have compared other approaches for the quantification of [^{11}C]FLB 457 binding, such as transient equilibrium and linear graphical analysis, and have shown that SRTM would produce the least biased estimates of BP_{ND}.[14–16] The aim of this study was to examine the degree of underestimation of BP_{ND} in amphetamine challenge studies, and the sensitivity for detecting amphetamine-induced dopamine release, as compared with an arterial input model method. The lack of change in cerebellum V_T and V_T/f_P pre- to postamphetamine helps validate the use of the cerebellum in amphetamine challenge studies, since the lack of amphetamine effect in the cerebellum avoids adding an extra bias and variability to $\%\Delta BP_{ND}$. Moreover, the low and consistent bias between 2TC and SRTM2 BP_{ND} estimates in the two conditions, and the lower variability of SRTM(2) BP_{ND} estimates compared with 2TC, further validates the use of reference region modeling approaches for future amphetamine challenge studies with [^{11}C]FLB 457 and PET.

Limitations

Data from six tobacco-smoking subjects were compared for the analysis of reference region input modeling approaches for amphetamine challenge studies with [^{11}C]FLB 457. One limitation of the study is the small sample size, but with SRTM and SRTM2 we were able to detect significant reductions in BP_{ND} postamphetamine across regions that were consistent with another study.[6] Another possible drawback of this study is the variability in $\%\Delta BP_{ND}$ between tobacco-smoking subjects. Variability among subjects may have been attributed to smoking habit. To examine this, number of pack years (number of cigarettes smoked per day × number of years smoked/20) was computed for all subjects with a mean ± s.d. of 14 ± 7. Regression analysis was performed, and there were no significant correlations between pack years and reduction in BP_{ND}(SRTM) nor BP_{ND}(SRTM2), averaged across ROIs. In addition, the variability is comparable to that previously reported in a larger group of 12 healthy control subjects.[6,7]

CONCLUSION

These data support the sensitivity of [^{11}C]FLB 457 and PET with SRTM and SRTM2 to detect amphetamine-induced dopamine release in extrastriatal regions in tobacco smokers. No changes in distribution volume were observed in the cerebellum. Both SRTM and SRTM2 can be used to estimate [^{11}C]FLB 457 BP_{ND} across brain regions with lower variability and consistent bias across baseline and amphetamine conditions, with lower bias in BP_{ND} with SRTM2, compared with 2TC. Thus, the need for arterial input data for future amphetamine challenge studies is not strictly required.

DISCLOSURE/CONFLICT OF INTEREST

The authors declare no conflict of interest.

ACKNOWLEDGMENTS

The authors would like to thank Erin McGovern, Evgenia Perkins, Ansel Hillmer and the staff at the Yale PET Center.

REFERENCES

1 Di Chiara G, Imperato A. Drugs abused by humans preferentially increase synaptic dopamine concentrations in the mesolimbic system of freely moving rats. *Proc Natl Acad Sci USA* 1988; **85**: 5274–5278.
2 Cardenas L, Houle S, Kapur S, Busto UE. Oral D-amphetamine causes prolonged displacement of [11C]raclopride as measured by PET. *Synapse* 2004; **51**: 27–31.
3 Gallezot JD, Kloczynski T, Weinzimmer D, Labaree D, Zheng MQ, Lim K *et al*. Imaging nicotine- and amphetamine-induced dopamine release in rhesus monkeys with [(11)C]PHNO vs [(11)C]raclopride PET. *Neuropsychopharmacology* 2014; **39**: 866–874.
4 Laruelle M. Imaging synaptic neurotransmission with in vivo binding competition techniques: a critical review. *J Cereb Blood Flow Metab* 2000; **20**: 423–451.
5 Narendran R, Jedema HP, Lopresti BJ, Mason NS, Gurnsey K, Ruszkiewicz J *et al*. Imaging dopamine transmission in the frontal cortex: a simultaneous microdialysis and [11C]FLB 457 PET study. *Mol Psychiatry* 2014; **19**: 302–310.
6 Narendran R, Frankle WG, Mason NS, Rabiner EA, Gunn RN, Searle GE *et al*. Positron emission tomography imaging of amphetamine-induced dopamine release in the human cortex: a comparative evaluation of the high affinity dopamine D2/3 radiotracers [11C]FLB 457 and [11C]fallypride. *Synapse* 2009; **63**: 447–461.
7 Narendran R, Himes M, Mason NS. Reproducibility of post-amphetamine [11C]FLB 457 binding to cortical D2/3 receptors. *PLoS One* 2013; **8**: e76905.
8 Innis RB, Cunningham VJ, Delforge J, Fujita M, Gjedde A, Gunn RN *et al*. Consensus nomenclature for in vivo imaging of reversibly binding radioligands. *J Cereb Blood Flow Metab* 2007; **27**: 1533–1539.
9 Lammertsma AA, Hume SP. Simplified reference tissue model for PET receptor studies. *Neuroimage* 1996; **4**: 153–158.
10 Asselin MC, Montgomery AJ, Grasby PM, Hume SP. Quantification of PET studies with the very high-affinity dopamine D2/D3 receptor ligand [11C]FLB 457: re-evaluation of the validity of using a cerebellar reference region. *J Cereb Blood Flow Metab* 2007; **27**: 378–392.

11 Ito H, Arakawa R, Takahashi H, Takano H, Okumura M, Otsuka T *et al.* No regional difference in dopamine D2 receptor occupancy by the second-generation antipsychotic drug risperidone in humans: a positron emission tomography study. *Int J Neuropsychopharmacol* 2009; **12**: 667–675.
12 Montgomery AJ, Asselin MC, Farde L, Grasby PM. Measurement of methylphenidate-induced change in extrastriatal dopamine concentration using [11C]FLB 457 PET. *J Cereb Blood Flow Metab* 2007; **27**: 369–377.
13 Narendran R, Mason NS, Chen CM, Himes M, Keating P, May MA *et al.* Evaluation of dopamine D(2)/(3) specific binding in the cerebellum for the positron emission tomography radiotracer [(1)(1)C]FLB 457: implications for measuring cortical dopamine release. *Synapse* 2011; **65**: 991–997.
14 Ito H, Sudo Y, Suhara T, Okubo Y, Halldin C, Farde L *et al.* Error analysis for quantification of [(11)C]FLB 457 binding to extrastriatal D(2) dopamine receptors in the human brain. *Neuroimage* 2001; **13**: 531–539.
15 Olsson H, Halldin C, Swahn CG, Farde L. Quantification of [11C]FLB 457 binding to extrastriatal dopamine receptors in the human brain. *J Cereb Blood Flow Metab* 1999; **19**: 1164–1173.
16 Olsson H, Farde L. Potentials and pitfalls using high affinity radioligands in PET and SPET determinations on regional drug induced D2 receptor occupancy--a simulation study based on experimental data. *Neuroimage* 2001; **14**: 936–945.
17 Suhara T, Sudo Y, Okauchi T, Maeda J, Kawabe K, Suzuki K *et al.* Extrastriatal dopamine D2 receptor density and affinity in the human brain measured by 3D PET. *Int J Neuropsychopharmacol* 1999; **2**: 73–82.
18 Hilton J, Yokoi F, Dannals RF, Ravert HT, Szabo Z, Wong DF *et al.* Column-switching HPLC for the analysis of plasma in PET imaging studies. *Nucl Med Biol* 2000; **27**: 627–630.
19 Viola P, Wells WM. Alignment by maximization of mutual information. *Int J Comput Vis*1997; **24**: 137–154.
20 Holmes CJ, Hoge R, Collins L, Woods R, Toga AW, Evans AC *et al.* Enhancement of MR images using registration for signal averaging. *J Comput Assist Tomogr* 1998; **22**: 324–333.
21 Tzourio-Mazoyer N, Landeau B, Papathanassiou D, Crivello F, Etard O, Delcroix N *et al.* Automated anatomical labeling of activations in SPM using a macroscopic anatomical parcellation of the MNI MRI single-subject brain. *Neuroimage* 2002; **15**: 273–289.
22 Petrides M, Pandya DN. Dorsolateral prefrontal cortex: comparative cytoarchitectonic analysis in the human and the macaque brain and corticocortical connection patterns. *Eur J Neurosci* 1999; **11**: 1011–1036.
23 Gunn RN, Gunn SR, Cunningham VJ. Positron emission tomography compartmental models. *J Cereb Blood Flow Metab* 2001; **21**: 635–652.
24 Wu Y, Carson RE. Noise reduction in the simplified reference tissue model for neuroreceptor functional imaging. *J Cereb Blood Flow Metab* 2002; **22**: 1440–1452.
25 Buck A, Westera G, vonSchulthess GK, Burger C. Modeling alternatives for cerebral carbon-11-iomazenil kinetics. *J Nucl Med* 1996; **37**: 699–705.
26 Pajevic S, Daube-Witherspoon ME, Bacharach SL, Carson RE. Noise characteristics of 3-D and 2-D PET images. *IEEE transactions on medical imaging* 1998; **17**: 9–23.
27 Parsey RV, Slifstein M, Hwang DR, Abi-Dargham A, Simpson N, Mawlawi O *et al.* Validation and reproducibility of measurement of 5-HT1A receptor parameters with [carbonyl-11C]WAY-100635 in humans: comparison of arterial and reference tisssue input functions. *J Cereb Blood Flow Metab* 2000; **20**: 1111–1133.
28 Slifstein M, Parsey RV, Laruelle M. Derivation of [(11)C]WAY-100635 binding parameters with reference tissue models: effect of violations of model assumptions. *Nucl Med Biol* 2000; **27**: 487–492.

Supplementary Information accompanies the paper on the Journal of Cerebral Blood Flow & Metabolism website (http://www.nature.com/jcbfm)